

Interfacial Tuning of Anisotropic Gilbert Damping


L. Chen^{1,*}, S. Mankovsky^{1b}, M. Kronseder³, D. Schuh³, M. Prager^{1b,3}, D. Bougeard³, H. Ebert²,
D. Weiss³, and C. H. Back^{1,4}

¹*Department of Physics, Technical University of Munich, Munich, Germany*

²*Department of Chemistry, Ludwig Maximilian University, Munich, Germany*

³*Institute of Experimental and Applied Physics, University of Regensburg, Regensburg, Germany*

⁴*Center for Quantum Engineering (ZQE), Technical University of Munich, Munich, Germany*

 (Received 31 July 2022; revised 17 October 2022; accepted 9 January 2023; published 27 January 2023)

Tuning of the anisotropic Gilbert damping $\Delta\alpha$ has been realized in ultrathin single-crystalline Fe films grown on GaAs (001). A nonmonotonic dependence of $\Delta\alpha$ on film thickness t is observed upon varying t about 10 ML (~ 1.4 nm). $\Delta\alpha$ increases for $16 \text{ ML} > t > 8.5 \text{ ML}$, and then decreases for $8.5 \text{ ML} > t > 6.5 \text{ ML}$ accompanied by a sign reversal of $\Delta\alpha$ for $t = 6.5 \text{ ML}$. The sign reversal of $\Delta\alpha$ is captured by first-principle calculations, which show that the anisotropic density of states changes sign upon decreasing t . Moreover, t^{-1} dependence of the anisotropic damping indicates the emergence of an anisotropic effective spin mixing conductance according to the theory of spin pumping. The results establish new opportunities for controlling the Gilbert damping and for fundamental studies of magnetization dynamics in reduced dimension.

DOI: [10.1103/PhysRevLett.130.046704](https://doi.org/10.1103/PhysRevLett.130.046704)

The study of the phenomenological Gilbert damping constant α occurring in the Landau-Lifshits-Gilbert equation has drawn significant interest since α is one of the fundamental parameters describing the dynamics of ferromagnetic materials [1]. Over the past decades, a large effort has been devoted to the understanding of the microscopic origin of α in bulk ferromagnets (FM) [2–7]. However, there are still many important questions concerning how damping evolves in quasi-two-dimensional systems, where at least one dimension is comparable to the electron mean free path [8].

From a technological point of view, α determines the critical current as well as the speed of current-induced magnetization switching in magnetic tunnel junctions [9–11] and in FM/heavy metal (HM) hybrids [12,13]. To optimize device performances, it is therefore highly desirable to find reliable and efficient means to design and control α , e.g., by electric fields [14] or by electric currents [15]. Besides these successful approaches for manipulation of α , spin pumping is known to enhance α of the FM due to the transfer of spin angular momentum from FM into the adjacent HM [16–18]. Quantitatively, the enhancement of α by spin pumping is [19,20]

$$\alpha = \alpha_0 + g_{\text{eff}}^{\uparrow\downarrow} \frac{\gamma\hbar}{4\pi M} t^{-1}, \quad (1)$$

where α_0 is the intrinsic damping of the FM, $\gamma (= g\mu_B/\hbar)$ the gyromagnetic ratio, g the Landé g factor, μ_B the Bohr's magneton, \hbar the reduced Planck constant, M the saturation magnetization, t the thickness of FM, and $g_{\text{eff}}^{\uparrow\downarrow}$ the effective

spin mixing conductance quantifying the spin pumping efficiency. Microscopically, $g_{\text{eff}}^{\uparrow\downarrow}$ is expressed in terms of spin-dependent reflection and transmission coefficients for electronic states at the FM/HM interface [21–23]. $g_{\text{eff}}^{\uparrow\downarrow}$ is also an important parameter describing interfacial spin transport in FM/HM bilayers [24], where the electronic band structure changes abruptly at the interface. For example, $g_{\text{eff}}^{\uparrow\downarrow}$ quantifies the interfacial spin transparency and is directly related to the accurate determination of the spin Hall angle of HMs in mutual spin-charge conversion experiments, e.g., spin pumping and electrical detection of the inverse spin Hall effect, spin Seebeck effect, spin Hall magnetoresistance and spin-torque experiments [25]. Equation (1) predicts that the damping enhancement is inversely proportional to t , indicating that spin pumping is an interfacial effect. Practically, $g_{\text{eff}}^{\uparrow\downarrow}$ can be determined by measuring the t dependence of α , and $g_{\text{eff}}^{\uparrow\downarrow}$ is determined to be around 10^{19} m^{-2} for various FM/HM interfaces [20,25]. Beside HMs, it has been shown theoretically and experimentally that other magnetically ordered materials, i.e., ferromagnets [26–30] and antiferromagnets [31–33], can also be effective spin sinks, showing the same order of magnitude of $g_{\text{eff}}^{\uparrow\downarrow}$ as HMs. So far, all results show that (i) $g_{\text{eff}}^{\uparrow\downarrow}$ is isotropic, (ii) once the interface is determined, there are no effective means to manipulate $g_{\text{eff}}^{\uparrow\downarrow}$.

Previously, we showed that, by exploring the interfacial spin-orbit interaction SOI at a single-crystalline Fe/GaAs (001) interface, anisotropic damping with twofold symmetry emerges [34], which provides the possibility to

observe an anisotropic $g_{\text{eff}}^{\uparrow\downarrow}$. Recently, it was shown that single-crystalline CoFe films host a giant damping anisotropy ($\Delta\alpha \sim 400\%$) with fourfold symmetry originating from the bulk anisotropic SOI [35] (an alternative interpretation is the anisotropic momentum relaxation time according to Ref. [36]). Since it is bulk related, it is difficult to manipulate $\Delta\alpha$. Here, we report the emergence of anisotropic $g_{\text{eff}}^{\uparrow\downarrow}$ in ultrathin Fe/GaAs films as well as a robust tuning of $\Delta\alpha$ and $g_{\text{eff}}^{\uparrow\downarrow}$ by interface engineering, i.e., by only varying the Fe thickness by a few monolayers (ML, 1 ML = 0.1435 nm). By changing t from 16 ML to 8.5 ML, we observe a progressive increase of $\Delta\alpha$ which is accompanied by an emerging anisotropic $g_{\text{eff}}^{\uparrow\downarrow}$. Moreover, by tuning t from 8.5 to 6.5 ML, $\Delta\alpha$ decreases and even a sign reversal of $\Delta\alpha$ is observed for $t = 6.5$ ML. The sign reversal of $\Delta\alpha$ is thus accompanied by a sign reversal of the anisotropic damping is captured by first-principles calculations, which show that the anisotropy of the density of states at the Fermi level—which is related to the damping parameter—changes sign upon decreasing t . Our results show that the interplay between confinement, dimensionality, interface-surface hybridization can provide an effective means for tuning Gilbert damping, ultimately leading to an exquisite control of spin dynamics [8].

To examine the effect of the interfacial states on anisotropic damping and the effective spin mixing conductance, single-crystalline Fe/GaAs samples are grown by molecular-beam epitaxy (MBE). For a better comparison of physical properties, samples with various Fe nominal thicknesses ($t = 6.5, 7, 7.5, 8, 8.5, 9, 10, 14,$ and 16 ML) are grown on a single two-inch wafer by stepping the main shadow shutter of the MBE. All samples are capped by 3 nm Al to avoid the oxidation of Fe and then are patterned into $30 \times 60 \mu\text{m}$ stripes. We use spin-orbit ferromagnetic resonance (SOFMR) [37,38] to measure the damping because (i) SOFMR facilitates the detection of the magnetization dynamics of ultrathin films with superior sensitivity since sizable spin-orbit torques arise at the Fe/GaAs interface [39], (ii) largely avoids the extrinsic effects to the damping due to a much-reduced detection area. All the devices are patterned along the [010] orientation to guarantee a sizable voltage signal along both the [110] ($\varphi_M = \varphi_H = 45^\circ$) and $[\bar{1}10]$ ($\varphi_M = \varphi_H = 135^\circ$) directions, where the magnitude of α takes extreme values [34]. Here, φ_M (φ_H) is the angle between magnetization \mathbf{M} (magnetic-field \mathbf{H}) and the [100] direction of GaAs as shown in Fig. 1(a). Figure 1(b) shows a typical dc voltage spectrum for $t = 8.5$ ML measured at a fixed microwave frequency f of 9 GHz and at room temperature. The voltage trace can be well fitted by combining a symmetric ($L_{\text{sym}} = \Delta H^2 / [4(H - H_R)^2 + \Delta H^2]$) and an antisymmetric Lorentzian ($L_{\text{a-sym}} = -4\Delta H(H - H_R) / [4(H - H_R)^2 + \Delta H^2]$), $V - V_{\text{offset}} = V_{\text{sym}}L_{\text{sym}} + V_{\text{a-sym}}L_{\text{a-sym}}$, where

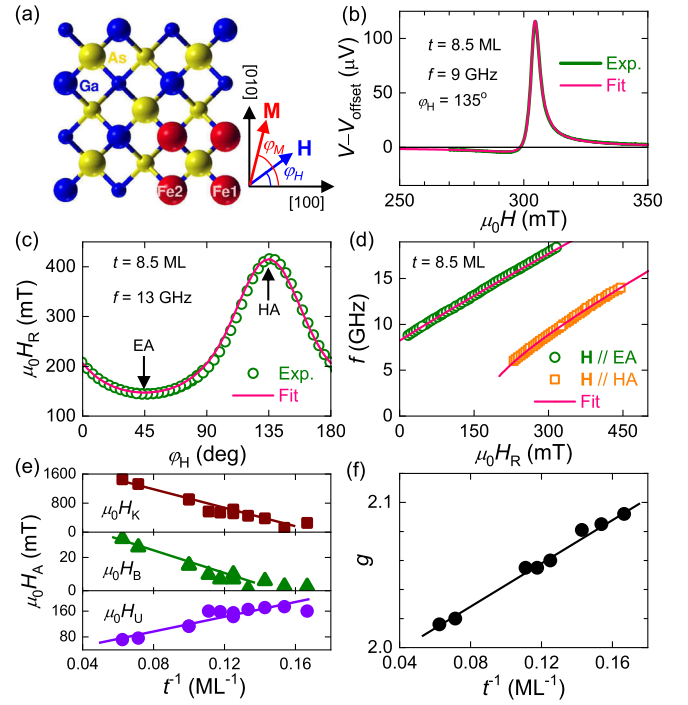


FIG. 1. (a) Top view of the anisotropic atomic bonding at the Fe/GaAs (001) interface. (b) Voltage trace for $t = 8.5$ ML measured at $f = 9$ GHz. The solid line is the fit from which the magnitude of H_R and ΔH are obtained. (c) φ_H dependence of H_R for $t = 8.5$ ML measured at $f = 13$ GHz. The solid line is the fit. The arrows point to the positions of EA and HA. (d) H_R dependence of f for $t = 8.5$ ML. Open circles represent \mathbf{H} along EA and open squares represent \mathbf{H} along HA. The solid lines are fits using the same parameters as (c). (e) t^{-1} dependence of H_K , H_B , and H_U . (f) t^{-1} dependence of the g factor. The solid lines in (e) and (f) are guides to the eyes.

V_{offset} is the offset voltage, H_R the H at FMR, ΔH the full width at half maximum, and V_{sym} ($V_{\text{a-sym}}$) the magnitude of the symmetric (antisymmetric) component of the dc voltage. The fitting gives values for V_{sym} , $V_{\text{a-sym}}$, H_R , and ΔH . In this work, we focus on the analysis of H_R and ΔH , related to magnetic anisotropies and damping, respectively.

A typical angular dependence of H_R for $t = 8.5$ ML, measured at $f = 13$ GHz is shown in Fig. 1(c). The sample shows typical uniaxial magnetic anisotropy (UMA) with twofold symmetry, i.e., a magnetically hard axis (HA) for $\varphi_M = 135^\circ$ and a magnetically easy axis (EA) for $\varphi_M = 45^\circ$, which originates from the anisotropic bonding at the Fe/GaAs interface [Fig. 1(a)]. The same behavior has been observed for all samples. To quantify the magnetic anisotropies, we further measure the f dependence of H_R both along EA and HA as shown in Fig. 1(d). Both angular and frequency dependence of H_R are fitted by [40]

$$\left(\frac{2\pi f}{\gamma}\right)^2 = \mu_0^2 H_1^R H_2^R, \quad (2)$$

with $H_1^R = H^R \cos(\varphi_M - \varphi_H) + H_K + H_B(3 + \cos 4\varphi_M)/4 - H_U \sin^2(\varphi_M - 45^\circ)$, and $H_2^R = H^R \cos(\varphi_M - \varphi_H) + H_B \cos 4\varphi_M - H_U \sin 2\varphi_M$. Here, H_K is the effective perpendicular magnetic anisotropy field including the demagnetization field, H_B the biaxial magnetic anisotropy field along $\langle 100 \rangle$, and H_U the in-plane UMA field along $[110]$. From the fits, the magnetic anisotropy fields H_A ($H_A = H_K, H_B, H_U$) and g for each t is obtained, and their dependences on the inverse Fe thickness t^{-1} are summarized in Figs. 1(e) and 1(f). Both H_K and H_B decrease as t decreases due to the reduced magnetization. However, H_U increases quasilinearly as t decreases, indicating an interfacial origin of UMA, which has also been observed previously [41,42]. Similar to H_U , g increases as t decreases, which is due to an enhanced orbital magnetic moment through a loss of bonds [43,44] and/or an enhanced sensitivity to the interfacial SOI as t decreases. To reproduce the φ_H and f dependence of H_R shown in Figs. 1(c) and 1(d), we use an isotropic g factor as there is no need to consider anisotropic g factors (or anisotropic γ values) in the data analysis.

Having analyzed t dependence of magnetic anisotropies, we turn to magnetic damping. Figure 2 shows the dependence of ΔH on f for representative t of 16, 8.5, 7, and 6.5 ML. Linear relations are observed for all samples, and α along HA and EA can be, respectively, determined from

$$\mu_0 \Delta H = 2\alpha(2\pi f/\gamma) + \mu_0 \Delta H_0, \quad (3)$$

where ΔH_0 is the zero-frequency intercept. For $t = 16$ ML shown in Fig. 2(a), the slopes along HA and EA are basically the same, indicating isotropic damping, i.e., $\alpha_{EA} \sim \alpha_{HA}$. As t reduces to 8.5 ML [Fig. 2(b)], a larger

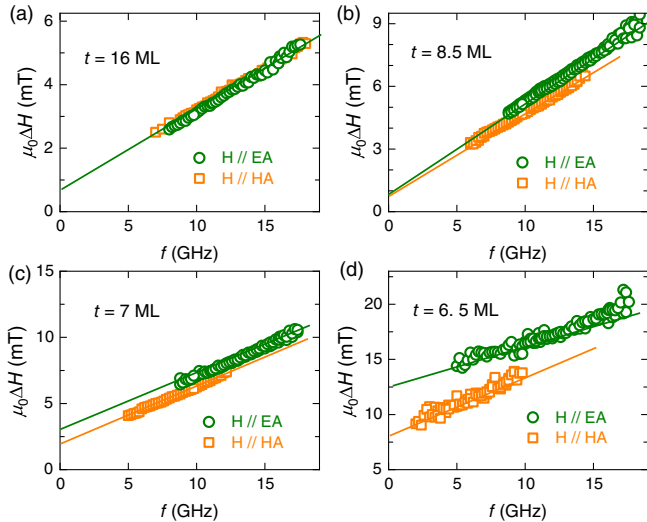


FIG. 2. f dependence of ΔH for $t = 16$ ML (a), 8.5 ML (b), 7 ML (c), and 6.5 ML (d). In (a)–(d), open circles represent \mathbf{H} along EA, and open squares represent \mathbf{H} along HA. The solid lines are fits from which α_{EA} and α_{HA} are obtained.

slope is seen along EA, pointing to the emergence of anisotropic damping with $\alpha_{EA} > \alpha_{HA}$, which is consistent with a previous report [34,45]. Interestingly, for $t = 7$ ML [Fig. 2(c)], the damping becomes isotropic again. As t further reduces to 6.5 ML [Fig. 2(d)], the slope along HA is larger, representing a sign reversal of the anisotropic damping, i.e., $\alpha_{EA} < \alpha_{HA}$. Apart from the slopes, ΔH_0 increases as t decreases with $\Delta H_0(EA) > \Delta H_0(HA)$, which is probably caused by enhanced electron-magnon scattering. We confirm that ΔH is primarily induced by intrinsic damping because (i) the φ_H dependence of ΔH has twofold symmetry, which can be well fitted by considering intrinsic damping [46]. (ii) the extrinsic effects, e.g., two-magnon scattering (TMS) and mosaicity broadening [49,50], can be excluded by additional in-plane to out-plane measurement [34].

The obtained damping parameters as a function of t^{-1} , i.e., α_{EA} and α_{HA} for all measured samples, are summarized in Fig. 3(a). In the subnanometer regime, α is of the lowest value, indicating the high quality of the samples [46]. Both α_{EA} and α_{HA} increase linearly as t decreases in regime I ($8.5 \text{ ML} < t < 16 \text{ ML}$) and regime II ($6.5 \text{ ML} < t < 8.5 \text{ ML}$), where regimes I and II are highlighted by the rectangular boxes. The linear dependence of damping on t^{-1} correlates the UMA and indicates the interfacial origin of damping. Since the dependence is linear (even for the smallest t), the contribution from TMS can be further excluded. This is different from the nonlinear t^{-1} dependence of α measured in polycrystalline FM/HM bilayer in which TMS, originating from spin-memory loss at the FM/HM interface, dominates the damping [25]. The damping anisotropy, $\Delta\alpha = (\alpha_{EA} - \alpha_{HA})/\alpha_{HA}$, is presented in the inset of Fig. 3(a). $\Delta\alpha$ increases as t decreases from 16 ML and reaches a maximum value of 22% for $t = 8.5$ ML. The maximal $\Delta\alpha$ is about 3 times smaller

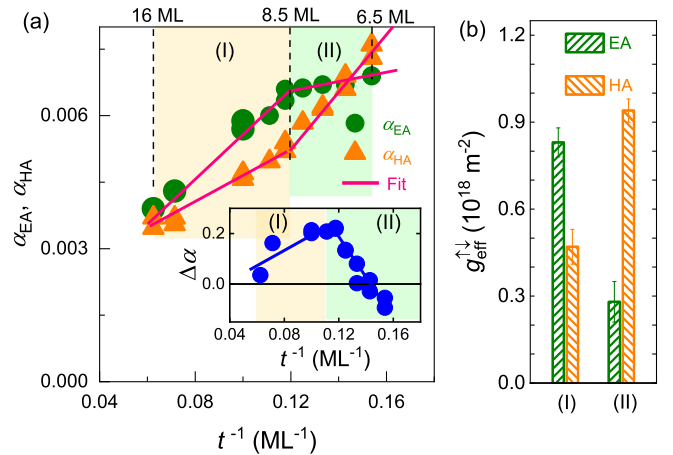


FIG. 3. (a) t^{-1} dependence of α_{EA} and α_{HA} . The inset shows the damping anisotropy $\Delta\alpha$ as a function of t^{-1} . The error bar is smaller than the symbol size. (b) Magnitude of $g_{\text{eff}}^{\uparrow\downarrow}$ along EA and HA in regimes I and II.

than Cr/Fe/GaAs samples [45]. The increase of $\Delta\alpha$ in regime I can be explained by an increased influence of interfacial SOI upon Fe. However, as t decreases further starting from 8.5 ML in regime II, $\Delta\alpha$ decreases and shows a sign reversal for $t = 6.5$ ML. Note that the total variation of t is only about 10 ML (~ 1.4 nm), demonstrating a robust tuning of the damping anisotropy by interface engineering.

The fact that α_{EA} and α_{HA} scale linearly with t^{-1} but with different slopes in regimes I and II suggests an emerging anisotropic effective spin mixing conductance. In regime I, the slope along the EA is larger than that along the HA, i.e., $k_{\text{EA}}^I > k_{\text{HA}}^I$, corresponding to a larger $g_{\text{eff}}^{\uparrow\downarrow}$ along the EA. However, a larger slope along the HA is observed in regime II, and $k_{\text{EA}}^{\text{II}} > k_{\text{HA}}^{\text{II}}$ holds, corresponding to a larger $g_{\text{eff}}^{\uparrow\downarrow}$ along the HA. The magnitude of $g_{\text{eff}}^{\uparrow\downarrow}$ calculated by Eq. (1) is shown in Fig. 3(b), which shows a sign reversal of $g_{\text{eff}}^{\uparrow\downarrow}$ in regimes I and II. The magnitude of $g_{\text{eff}}^{\uparrow\downarrow}$ is about one order smaller than that in HM/FM bilayers, probably due to a weaker SOI at the Fe/GaAs interface. Since the damping anisotropy is induced by the anisotropic electron density, and the emergence of anisotropic $g_{\text{eff}}^{\uparrow\downarrow}$ could be induced by anisotropic scattering at the Fe/GaAs interface, which hasn't been described theoretically so far. The anisotropic $g_{\text{eff}}^{\uparrow\downarrow}$ could lead to various anisotropic phenomena in HM/Fe/GaAs heterostructures, i.e., magnetization-direction-dependent inverse spin Hall voltage induced by spin pumping, spin Hall magnetoresistance, unidirectional magnetoresistance and spin torques. It also implies that the critical current for magnetization switching or for the auto-oscillation of magnetizations can be simply controlled by applying current along different directions in the same device [35], providing an alternative chance for device optimization.

Finally, we discuss the mechanism for the sign reversal of the anisotropic damping. As discussed in Refs. [4–7], α in metallic systems is primarily determined by electronic states at the Fermi level E_F . It is expected that the layer-resolved electronic structure of Fe layer, being sufficiently distant from the interface, has fourfold symmetry, following the symmetry of the crystal structure of bcc Fe. However, at the interface, this fourfold symmetry is reduced to twofold because of the anisotropic bonding to GaAs. The reduced structural symmetry at the interface is therefore expected to influence the electronic states and thus damping. The spatial symmetry of the layer-resolved anisotropic structure determines its SOI-driven modification upon magnetization rotation, leading in turn to a modified electronic states and damping, being different at the interface, the surface, or in the middle of film. Here, the Bychkov-Rashba (BR) SOI of the interface and surface layers differs because of a different charge distribution around the interface and the surface. The layer-resolved anisotropic density of states and the layer-resolved Bloch spectral function obtained from first-principle calculations

support this scenario [46]. Figure 4(a) shows the φ_M dependence of the total anisotropic density of states (ADOS, ΔN) at E_F , $\Delta N = N(E_F, \varphi_M) - N(E_F, \varphi_M = 45^\circ)$, for t ranging from 9 to 2 ML. For $t = 9$ ML, a larger DOS is observed for $\mathbf{M} \parallel [110]$ with ΔN reaching -1.38 states/Ry, corresponding to $\alpha_{\text{EA}} > \alpha_{\text{HA}}$. The twofold symmetry of the ADOS reflects the interference of BR and Dresselhaus SOI at the Fe/GaAs interface [39,51]. As t decreases (e.g., $t = 5$ and 3 ML), the magnitude of ΔN decreases. Interestingly, when t reaches 2 ML, a larger DOS appears for $\mathbf{M} \parallel [\bar{1}10]$. This can be attributed to a strong modification of the electronic structure at the interface when t decreases. The sign reversal of the ADOS leads obviously to a sign reversal of the anisotropic damping with $\alpha_{\text{EA}} < \alpha_{\text{HA}}$ for the thinnest t .

Figure 4(b) shows the calculated damping anisotropy at room temperature. The damping anisotropy reaches a maximum around 6–9 ML and changes sign for $t = 2$ ML, consistent with the experimental observations. As shown in the inset, the damping along EA decreases faster than that along HA when t decreases from 5 to 2 ML. This may stem from a strong modification of the electronic structure of the interface layer for the 2 ML film due to strong hybridization of interface and surface states; in contrast to thicker films

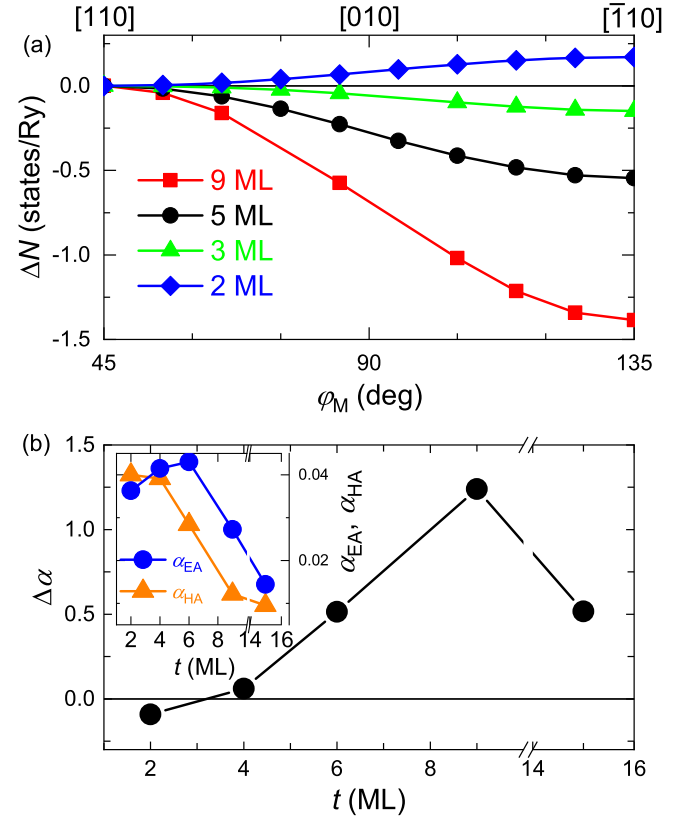


FIG. 4. (a) φ_M dependence of the calculated anisotropic electron density of states ΔN at the Fermi level for different t . (b) Calculated $\Delta\alpha$ as a function of t . The inset shows the calculated α_{EA} and α_{HA} as a function of t .

for which the interface electronic structure is only weakly modified when t changes. In calculation, a perfect interface has been assumed, resulting in a more pronounced—compared to experiment—damping anisotropy following the anisotropy of the electronic structure. In the experimental case, a certain interface roughness and partial intermixing cannot be avoided, leading to a significant isotropic interband contribution to damping and then a decreased damping anisotropy. Furthermore, the 2, 3, and 5 ML samples were all assumed to be ferromagnetic in calculation, while in experiment, the thinnest measurable thickness (with good crystallinity and ferromagnetic order at room temperature) is 6.5 ML [52]. In this case, a one-to-one comparison between experiment and theory is not possible. Therefore, in summary for the thinnest layers, the difference between theoretical results and experimental observation might stem from the details of the interface.

In summary, we have observed a sign reversal of the anisotropic damping as well as a sign reversal of the anisotropic effective spin mixing conductance in ultrathin Fe films grown on GaAs (001), when changing the thickness of the Fe. The sign reversal of the anisotropic damping by reducing the Fe thickness can be explained by the sign reversal of the anisotropic density of states. Our results identify the thickness as a key parameter for tuning and controlling the anisotropic damping and the spin mixing conductance in a quasi-two-dimensional system.

We would like to thank M. Stiles for fruitful discussions. This work is supported by the Deutsche Forschungsgemeinschaft (German Research Foundation), Project-ID 314695032—SFB 1277.

*Corresponding author.
lin0.chen@tum.de

- [1] T. L. Gilbert, *IEEE Trans. Magn.* **40**, 3443 (2004).
- [2] V. Kambarský, *Czech. J. Phys. B* **26**, 1366 (1976).
- [3] D. Thonig and J. Henk, *New. J. Phys.* **16**, 013032 (2014).
- [4] K. Gilmore, Y. U. Idzerda, and M. D. Stiles, *Phys. Rev. Lett.* **99**, 027204 (2007).
- [5] A. Brataas, Y. Tserkovnyak, and G. E. W. Bauer, *Phys. Rev. Lett.* **101**, 037207 (2008).
- [6] H. Ebert, S. Mankovsky, D. Ködderitzsch, and P. J. Kelly, *Phys. Rev. Lett.* **107**, 066603 (2011).
- [7] I. Garate and A. MacDonald, *Phys. Rev. B* **79**, 064404 (2009).
- [8] J. Pellicciari, S. Lee, K. Gilmore, J. Li, Y. Gu, A. Barbour, I. Jarrige, C. H. Ahn, F. J. Walker, and V. Bisogni, *Nat. Mater.* **20**, 188 (2021).
- [9] J. C. Slonczewski, *J. Magn. Magn. Mater.* **159**, L1 (1996).
- [10] L. Berger, *Phys. Rev. B* **54**, 9353 (1996).
- [11] D. C. Ralph and M. D. Stiles, *J. Magn. Magn. Mater.* **320**, 1190 (2008).
- [12] K. Lee, S. Lee, B. Min, and K. Lee, *Appl. Phys. Lett.* **102**, 112410 (2013).
- [13] A. Manchon, J. Železný, I. M. Miron, T. Jungwirth, J. Sinova, A. Thiaville, K. Garello, and P. Gambardella, *Rev. Mod. Phys.* **91**, 035004 (2019).
- [14] L. Chen, F. Matsukura, and H. Ohno, *Phys. Rev. Lett.* **115**, 057204 (2015).
- [15] K. Ando, S. Takahashi, K. Harii, K. Sasage, J. Ieda, S. Maekawa, and E. Saitoh, *Phys. Rev. Lett.* **101**, 036601 (2008).
- [16] Y. Tserkovnyak, A. Brataas, and G. E. W. Bauer, *Phys. Rev. Lett.* **88**, 116601 (2002).
- [17] Y. Tserkovnyak, A. Brataas, and G. E. W. Bauer, *Phys. Rev. B* **66**, 224403 (2002).
- [18] S. Mizukami, Y. Ando, and T. Miyazaki, *Phys. Rev. B* **66**, 104413 (2002).
- [19] M. Zwierzycki, Y. Tserkovnyak, P. J. Kelly, A. Brataas, and G. E. W. Bauer, *Phys. Rev. B* **71**, 064420 (2005).
- [20] C. F. Pai, Y. Ou, L. H. Vilela-Leão, D. C. Ralph, and R. A. Buhrman, *Phys. Rev. B* **92**, 064426 (2015).
- [21] A. Brataas, Y. V. Nazarov, and G. E. W. Bauer, *Phys. Rev. Lett.* **84**, 2481 (2000).
- [22] M. D. Stiles and A. Zangwill, *Phys. Rev. B* **66**, 014407 (2002).
- [23] K. Xia, P. J. Kelly, G. E. W. Bauer, A. Brataas, and I. Turek, *Phys. Rev. B* **65**, 220401(R) (2002).
- [24] V. P. Amin and M. D. Stiles, *Phys. Rev. B* **94**, 104419 (2016).
- [25] L. J. Zhu, D. C. Ralph, and R. A. Buhrman, *Phys. Rev. Lett.* **123**, 057203 (2019).
- [26] Y. Ohnuma, H. Adachi, E. Saitoh, and S. Maekawa, *Phys. Rev. B* **89**, 17417 (2014).
- [27] Y. Ou, D. C. Ralph, and R. A. Buhrman, *Phys. Rev. Lett.* **120**, 097203 (2018).
- [28] Y. Y. Wang, M. M. Decker, T. N. G. Meier, X. Chen, C. Song, T. Grünbaum, W. Zhao, J. Zhang, L. Chen, and C. H. Back, *Nat. Commun.* **11**, 275 (2020).
- [29] S. Varotto, M. Cosset-Chéneau, C. Grèzes, Y. Fu, P. Warin, A. Brenac, J. Jacquot, S. Gambarelli, C. Rinaldi, V. Baltz, J. Attané, L. Vila, and Paul Noël, *Phys. Rev. Lett.* **125**, 267204 (2020).
- [30] P. Wu, D. Qu, Y. Tu, Y. Lin, C. L. Chien, and S. Y. Huang, *Phys. Rev. Lett.* **128**, 227203 (2022).
- [31] L. Frangou, S. Oyarzún, S. Auffret, L. Vila, S. Gambarelli, and V. Baltz, *Phys. Rev. Lett.* **116**, 077203 (2016).
- [32] Z. Qiu, J. Li, D. Hou, E. Arenholz, A. T. N'Diaye, A. Tan, K. Uchida, K. Sato, S. Okamoto, Y. Tserkovnyak, Z. Q. Qiu, and E. Saitoh, *Nat. Commun.* **7**, 12670 (2016).
- [33] L. J. Zhu, L. J. Zhu, and R. A. Buhrman, *Phys. Rev. Lett.* **126**, 107204 (2021).
- [34] L. Chen, S. Mankovsky, S. Wimmer, M. A. W. Schoen, H. S. Körner, M. Kronseder, D. Schuh, D. Bougeard, H. Ebert, D. Weiss, and C. H. Back, *Nat. Phys.* **14**, 490 (2018).
- [35] Y. Li, F. Zeng, S. S. L. Zhang, H. Shin, H. Saglam, V. Karakas, O. Ozatay, J. E. Pearson, O. G. Heinonen, Y. Wu, A. Hoffmann, and W. Zhang, *Phys. Rev. Lett.* **122**, 117203 (2019).
- [36] Y. Dai, Y. W. Zhao, L. Ma, M. Tang, X. P. Qiu, Y. Liu, Z. Yuan, and S. M. Zhou, *Phys. Rev. Lett.* **128**, 247202 (2022).
- [37] L. Chen, M. Decker, M. Kronseder, R. Islinger, M. Gmitra, D. Schuh, D. Bougeard, J. Fabian, D. Weiss, and C. H. Back, *Nat. Commun.* **7**, 13802 (2016).

- [38] D. Fang, H. Kurebayashi, J. Wunderlich, K. Výborný, L. P. Zârbo, R. P. Campion, A. Casiraghi, B. L. Gallagher, T. Jungwirth, and A. J. Ferguson, *Nat. Nanotechnol.* **6**, 413 (2011).
- [39] L. Chen, R. Islinger, J. Stigloher, M. M. Decker, M. Kronseder, D. Schuh, D. Bougeard, D. Weiss, and C. H. Back, *Phys. Rev. B* **104**, 014425 (2022).
- [40] L. Chen, F. Matsukura, and H. Ohno, *Nat. Commun.* **4**, 2055 (2013).
- [41] G. Bayreuther, J. Prempfer, M. Sperl, and D. Sander, *Phys. Rev. B* **86**, 054418 (2009).
- [42] G. Bayreuther, M. Dumm, B. Uhl, R. Meier, and W. Kipferl, *J. Appl. Phys.* **93**, 8230 (2003).
- [43] J. M. Shaw, R. Knut, A. Armstrong, S. Bhandary, Y. Kvashnin, D. Thonig, E. K. Delczeg-Czirjak, O. Karis, T. J. Silva, E. Weschke, H. T. Nembach, O. Eriksson, and D. A. Arena, *Phys. Rev. Lett.* **127**, 207201 (2021).
- [44] L. Giovanelli, G. Panaccione, G. Rossi, M. Fabriziooli, C. S. Tian, P. L. Gastelois, J. Fujii, and C. H. Back, *Appl. Phys. Lett.* **87**, 042506 (2005).
- [45] L. Yang, Y. Yan, Y. Chen, Y. Chen, B. Liu, Z. Chen, X. Lu, J. Wu, L. He, X. Ruan, B. Liu, and Y. Xu, *J. Phys. D* **53**, 115004 (2020).
- [46] See Supplemental Material at <http://link.aps.org/supplemental/10.1103/PhysRevLett.130.046704> for the analysis of angular dependence of linewidth, the summary of damping in ultrathin ferromagnets, and first-principle calculations, where Refs. [47,48] are also included.
- [47] G. Malinowski, K. C. Kuiper, R. Lavrijsen, H. J. M. Swagten, and B. Koopmans, *Appl. Phys. Lett.* **94**, 102501 (2009).
- [48] L. Bainsla *et al.*, *Adv. Funct. Mater.* **32**, 2111693 (2022).
- [49] R. Aerials and D. L. Mills, *Phys. Rev. B* **60**, 7395 (1999).
- [50] R. D. McMichael, D. J. Twisselmann, and A. Kunz, *Phys. Rev. Lett.* **90**, 227601 (2003).
- [51] M. Gmitra, A. Matos-Abiague, C. Draxl, and J. Fabian, *Phys. Rev. Lett.* **111**, 036603 (2013).
- [52] G. Wastlbauer and J. A. C. Bland, *Adv. Phys.* **54**, 137 (2005).